Final Report for NASA Grant

NAG9-946

submitted to

National Aeronautics and Space Administration
Lyndon B. Johnson Space Center
ATTN: Eric L. Christiansen
Space Science Branch, Code SN3
Houston, TX 77058

For Research Entitled

PARTICLE HYDRODYNAMICS WITH MATERIAL STRENGTH FOR MULTI-LAYER ORBITAL DEBRIS SHIELD DESIGN

by   ..

Eric P. Fahrenthold
Department of Mechanical Engineering
University of Texas
Austin, TX 78712

August 11, 1999

ABSTRACT

Three dimensional simulation of oblique hypervelocity impact on orbital debris shielding places extreme demands on computer resources. Research to date has shown that particle models provide the most accurate and efficient means for computer simulation of shield design problems. In order to employ a particle based modeling approach to the wall plate impact portion of the shield design problem, it is essential that particle codes be augmented to represent strength effects. This report describes augmentation of a Lagrangian particle hydrodynamics code developed by the principal investigator, to include strength effects, allowing for the entire shield impact problem to be represented using a single computer code.

TABLE OF CONTENTS

Page

CHAPTER 1: INTRODUCTION

This report describes work performed under NASA Grant NAG9-946 aimed at the development and validation of a new particle-element method for hypervelocity impact simulation. Chapter 2 describes the basic method and illustrates its application with two test problems. Chapter 3 describes a series of simulations conducted to validate the method for representative Whipple shield orbital debris shielding applications. (Chapters 2 and 3 are papers in press in the International Journal of Impact Engineering.) Chapter 4 describes additional test problems which simulate published hypervelocity impact experiments. The final chapter indicates directions for future work.

NOTE: References are listed at the end of each individual chapter.

CHAPTER 2: HYBRID PARTICLE-ELEMENT METHOD

--

A HYBRID PARTICLE-FINITE ELEMENT METHOD FOR HYPERVELOCITY IMPACT SIMULATION

ERIC P. FAHRENTHOLD and BLAISE A. HORBAN

Department of Mechanical Engineering, University of Texas, Austin, TX 78712

Summary—Coupled particle-finite element methods have been suggested as an approach to modeling particular impact problems not well suited to simulation with conventional Eulerian, Lagrangian, or particle codes. An alternative hybrid particle-finite element technique has been developed, in which particles are used to model contact-impact and volumetric deformation while finite elements are employed to represent interparticle tension forces and elastic-plastic deviatoric deformation. The method has been implemented in a three dimensional code and applied to simulate representative hypervelocity impact problems.

INTRODUCTION

Particle-based numerical impact models [1] can offer distinct advantages over Eulerian [2] and Lagrangian [3] hydrocodes in particular hypervelocity impact applications. An example is the design of orbital debris shielding [4, 5], where conventional codes have proven difficult to apply [6, 7, 8]. Particle models avoid certain problems with mesh distortion and debris transport which have hindered the effective use of Lagrangian and Eulerian codes in the simulation of three dimensional impacts on shielded space structures [9]. However particle methods typically incorporate kinematically inexact treatments of material history effects such as plasticity and fracture. Recent research efforts have been directed at the formulation of coupled particle-finite element methods for hypervelocity impact simulation [10], as well as a variety of other new numerical methods [11, 12].

Both particle-in-cell (PIC) methods [13] and smooth particle hydrodynamics (SPH) methods [14, 15] employ particles which are actually moving interpolation points. An alternative particle-based modeling methodology developed by Fahrenthold and Koo [16, 17] offers a fully Lagrangian, energy-based approach to shock physics simulations. This alternative approach, labeled Hamiltonian particle hydrodynamics, avoids the tensile and boundary instabilities associated with some smooth particle hydrodynamics formulations [18, 19] and the potentially diffusive grid-to-particle mapping schemes characteristic of some particle-in-cell methods.

In recent work, the particle method of Fahrenthold and Koo has been extended, by coupling the aforementioned hydrodynamic particle model to a Lagrangian finite element description of material strength in the continuum. The resulting hybrid particle-finite element model retains all of the features (including general contact-impact effects) of Hamiltonian particle hydrodynamics, while in addition accounting for tensile strength, elastic shearing strain, plasticity, and continuum damage effects important in the simulation of some hypervelocity impact problems.

The finite element kinematics used here are similar (not identical) to those employed in existing Lagrangian hydrocodes [20], for example DYNA3D [3]. The coordinates of certain nearest neighbor particles, identified in the reference configuration, determine finite element nodal displacements and hence the local elastic shearing strain, the local plastic strain rate, and interparticle tensile forces. Normal and deviatoric continuum damage variables are introduced to allow for perforation, fragmentation, and fracture in arbitrary geometry's, while no slideline

algorithms [21] are employed. Element failure is based on strictly physical criteria, and is not dependent on any smoothing length or mesh-to-particle mapping scheme. Unlike other particle based strength models, the present formulation incorporates exact Lagrangian finite strain kinematics, which have proven effective in Lagrangian finite element codes in characterizing highly strength dependent features of impact dynamics problems.

A three dimensional, parallel implementation of the hybrid numerical method described here has been coded, with specific interest in the application of orbital debris shielding design. The sections which follow outline the hybrid formulation, and illustrate the method using two example simulations with known experimental results.

MODELING METHODOLOGY

The hybrid particle-finite element model described here is formulated using an energy method, namely Hamiltonian mechanics [22]. Hence the model formulation procedure differs markedly from that used in weighted residual finite element techniques or the finite difference (finite volume) method. It differs also from the model formulation procedure used with many particle methods, which typically rely in part on energy concepts and in part on the differential balance equations for the continuum. As in all discrete Hamiltonian methods, the present model is formulated by assembling kinetic and potential energy expressions for the system, describing the relevant constraint equations, and introducing Lagrange multipliers, in order to arrive at the final first order state (evolution) equations for the system. Unlike the familiar and purely mechanical Hamiltonian models seen often in the literature, the present work employs entropy states to model the thermal dynamics of the system. One result is that the energy dissipation expression normally used to quantify viscous generalized forces is replaced by a set of nonholonomic constraints on the entropy evolution. These and other differences from classical Hamiltonian formulations are discussed in more detail by Fahrenthold and Koo [16, 17], who also employ a Hamiltonian methodology to formulate a particle model of the SPH type.

The sections which follow discuss the particle and element kinematics, the stored energy expressions for the system, and the nonholonomic constraints, and then apply Hamilton's canonical equations to arrive at a state space description of the impact dynamics problem. The particles are used to model kinetic energy effects, contact-impact, and thermomechanical volumetric deformation, while the finite elements represent strength effects (interparticle tension, elastic shear, and plastic deformation). Contact-impact is modeled using penalty forces similar to those employed in DYNA3D. Numerical viscosity is introduced to damp all the elastic modes, and numerical heat conduction serves to diffuse shock heating.

KINEMATICS

This section provides an overview of the particle and element kinematics. The particles of the present model are homogeneously deformed, spherical, Lagrangian control volumes. Hence their motion is described completely by a scalar deformation gradient (F) and a center of mass position vector (c) for each particle. The material time derivatives ($\dot{F}$ and $\dot{c}$) of these generalized coordinates are generalized velocities for the Hamiltonian system. In the reference (undeformed) configuration for the modeled system, the particles are arranged in a body-centered cubic packing scheme.

The Lagrangian finite elements used here incorporate nine nodes: they are eight-noded hexahedra, with a ninth node located (in the reference configuration) at the element centroid. Eight "edge centered" particles define the corners of a hexahedra, while a "body centered" particle locates the interior node. In other words, the particle center of mass coordinates are also nodal coordinates, for intact (uneroded) elements. Each element is subdivided into six separate five-noded subelements, by associating the body centered particle for each element with the six separate sets of four particles which define the faces of the hexahedron. The volumes of the subelements are used in calculating interparticle tensile forces, while the shear deformation of the hexahedron is used to determine the deviatoric strain. The hexahedra are used to describe the following

Lagrangian finite strain kinematics for the continuum. The elastic deviatoric strain tensor (E^e) for an element is defined by

$$E^e = \bar{E} - E^p \tag{1a}$$

where E^p is the plastic strain tensor, and the deviatoric total strain is [23]

$$\bar{E} = (1/2)(\bar{C} - I) \quad ; \quad \bar{C} = J^{-2/3} C; \quad J = [\det(C)]^{1/2} \tag{1b,c,d}$$

with J the Jacobian of the hexahedron and C the right Cauchy-Green strain tensor. Since the edge centered particles define the hexahedra, the center of mass coordinates for those particles are used to calculate the strain tensor (C) and element Jacobian (J). As a result the only new generalized coordinates (internal state variables) introduced by the elements are the six components of the symmetric plastic strain tensor (E^p) for each element.

KINETIC ENERGY

The kinetic energy (T) of the system is a function of the particle translation and deformation, and takes the form [16, 17]

$$T = (1/2) \sum_{i=1}^{n} [m^{(i)-1} p^{(i)2} + M^{(i)-1} H^{(i)2}] = T(p^{(i)}, H^{(i)}) \tag{2a}$$

where n is the number of particles, m is the particle mass, M is the (constant) particle moment of inertia in the reference configuration, p is the particle center of mass momentum, H is the particle distributed momentum, and the superscript "(i)" denotes the ith particle. The generalized momenta are related to the corresponding generalized velocities by

$$\dot{c}^{(i)} = \frac{\partial T}{\partial p^{(i)}} = m^{(i)-1} p^{(i)} \quad ; \quad \dot{F}^{(i)} = \frac{\partial T}{\partial H^{(i)}} = M^{(i)-1} H^{(i)}$$

(2b,c)

INTERNAL ENERGY

The conserved potential in this Hamiltonian model is the system internal energy (U). The internal energy is partitioned into three parts: (1) a thermomechanical potential (u, an internal energy per unit mass) for each particle which depends on the current particle density (ρ) and entropy per unit mass (s), (2) a deviatoric strain energy which depends on the elastic strain tensor (E^e) and a deviatoric damage variable (d, $0 \leq d \leq 1$), and (3) an interparticle tensile strain energy which depends on the particle deformation gradients, the subelement volumes, and a normal damage variable (D, $0 \leq D \leq 1$). Specifically

$$U = \{ \sum_{i=1}^{n} m^{(i)} u^{(i)}(\rho^{(i)}, s^{(i)}) \} + \{ \sum_{i=1}^{n_e} (1 - d^{(i)}) V_o^{e(i)} \mu^{(i)} E^{e(i)} : E^{e(i)} \} +$$

$$\{ \sum_{i=1}^{n_e} \sum_{j=1}^{6} (1/2)(1 - D^{(i)}) V_o^{e(i,j)} K^{(i)} < v^{e(i,j)} / V_o^{e(i,j)} - \vartheta^{(i,j)} >^2 \} \tag{3}$$

where n_e is the number of elements, $V_o^{e(i)}$ denotes the reference volume for element "i", $V^{e(i,j)}$ and $V_o^{e(i,j)}$ are the current and reference volume for subelement "j" of element "i", $\mu^{(i)}$ and $K^{(i)}$ are the shear modulus and the reference bulk modulus for element "i", $\vartheta^{(i,j)}$ is the mass weighted average of the particle Jacobians for subelement "j" of element "i", and the notation "< >" represents the Macauley bracket [$< x > = x$ for $x > 0$, $< x > = 0$ for $x \leq 0$]. In view of the aforementioned particle kinematics,

$$\vartheta^{(i,j)} = \vartheta^{(i,j)} (F^{(k)}) \quad ; \quad u^{(i)} = u^{(i)}(F^{(i)}, S^{(i)}) \quad ; \quad S^{(i)} = m^{(i)} s^{(i)}$$

(4a,b,c)

so that the total particle entropy (S) is a generalized coordinate for the system. Likewise, in view of the aforementioned element kinematics,

$$E^{e(i)} = E^{e(i)} (c^{(k)}, E^{p(i)}) \quad ; \quad V^{e(i,j)} = V^{e(i,j)} (c^{(k)})$$

(4d,e)

so that the total internal energy has the functional form

$$U = U (F^{(i)}, S^{(i)}, c^{(i)}, E^{p(i)}, D^{(i)}, d^{(i)})$$

(5a)

The corresponding generalized conservative forces are

$$G^{(i)} = \frac{\partial U}{\partial F^{(i)}} \quad ; \quad \theta^{(i)} = \frac{\partial U}{\partial S^{(i)}} \quad ; \quad g^{(i)} = \frac{\partial U}{\partial c^{(i)}}$$

(5b,c,d)

where $\theta^{(i)}$ is the temperature for particle "i", while

$$\Gamma^{(i)} = - \frac{\partial U}{\partial D^{(i)}} \quad ; \quad \eta^{(i)} = - \frac{\partial U}{\partial d^{(i)}}$$

(5e,f)

are energy release rates associated with normal and shear damage evolution and

$$S^{(i)} = 2\mu^{(i)} (1 - d^{(i)}) \ E^{e(i)} = - (1/V_o^{e(i)}) \frac{\partial U}{\partial E^{p(i)}}$$

(5g)

is a deviatoric stress tensor.

PLASTICITY MODEL

The plasticity model used here is a rate independent variation of the isochoric finite strain formulation of Fahrenthold and Horban [24]. The flow rule for the incremental plastic strain is taken as

$$\Delta E^p = \Delta \lambda \ W$$

(6a)

$$\Delta \lambda = < \tau - Y > / \{ 2\mu (1-d) \ [(1/2) \ W:W]^{1/2} \} \quad ; \quad \tau^2 = (1/2) \ S:S$$

(6b,c)

where τ is the effective shear stress, Y is the yield stress, and

$$W = C^p \ A' + A' \ C^p \tag{6d}$$

$$A' = A - (1/3) \ \mathrm{tr}(A) \ I \quad ; \quad A = S \ C^p + C^p \ S$$
(6e,f)

$$C^p = I + 2 \ E^p \tag{6g}$$

In general, the yield stress is taken to be a linear function of J and θ [25]. Here

$$Y = Y(J, \theta) = < \alpha \ J - 1 > \ < 1 - \beta \ (\theta - \theta_0)/(\theta_m - \theta_0) > Y_0$$
(7a)

where θ_0 and θ_m are a reference and melting temperature, Y_0 is a reference yield stress, and α and β are constants. For use in determining element failure, the effective plastic strain (ε^p) is tracked by integrating

$$\dot{\varepsilon}^p = [(1/2) (\dot{E}^p : \dot{E}^p)]^{1/2} \tag{7b}$$

It should be noted that the present modeling methodology allows for the introduction of alternative elastic-plastic formulations [26].

DAMAGE EVOLUTION EQUATIONS

The normal and shear damage variables serve to degrade the element moduli in shear and tension, and thereby represent the loss of cohesive strength associated with material failure. The energy released in damage evolution is a source of irreversible entropy production, so that no internal energy is discarded. The simple rate independent damage evolution relations used here are

$$\Delta D = \Delta d = \omega \quad ; \quad \omega = \text{constant (normally 0.1)} \tag{8}$$

for any time step after an element "fails", due to any one of several effects: (1) the (negative) tensile pressure drops below a specified value, (2) the effective shear stress exceeds a specified value, (3) the maximum eigenvalue of the deviatoric stress tensor exceeds a specified value, or (4) the accumulated plastic strain exceeds a specified value. For $\omega = 0.1$ element failure will occur gradually, over ten time steps [27]. Once the maximum damage value of 1.0 is reached, the element has lost all cohesion and ω is again set to zero.

It should be noted that nothing in the methodology described here precludes the implementation of more complex damage evolution models, like those previously implemented in particle based [28] or Eulerian [29] codes.

NUMERICAL VISCOSITY

Considering the preceding discussion of particle and element kinematics, numerical viscosity [30] is required to damp both relative motion of the particle mass centers and bulk deformation of the individual particles. The damping force on particle "i" due to relative particle motion is taken as

$$f^{(i)} = \sum_{j=1}^{n} v^{(i,j)} \ \{ (\dot{c}^{(i)} - \dot{c}^{(j)}) \cdot (c^{(i)} - c^{(j)}) \} (c^{(i)} - c^{(j)}) / (\dot{c}^{(i)} - \dot{c}^{(j)})^2$$
(9a)

where $v^{(i,j)}$ is the numerical viscosity

$$v^{(i,j)} = c_0 \, (1/2) \, (\rho^{(i)} \, c_s^{(i)} A^{(i)} + \rho^{(j)} \, c_s^{(j)} A^{(j)}) \; \Lambda[\zeta^{(i,j)}] \tag{9b}$$

$$\zeta^{(i,j)} = (h^{(i)} + h^{(j)}) - |c^{(i)} - c^{(j)}| \tag{9c}$$

with c_0 a dimensionless viscosity coefficient, $c_s^{(i)}$ the sound speed for particle "i", $A^{(i)}$ the cross sectional area for particle "i", $h^{(i)}$ the radius for particle "i", and $\Lambda[\zeta]$ a step function ensuring that only neighboring particles interact

$$\Lambda[\zeta] = 1 \text{ for } \zeta \geq 0 \; ; \; \Lambda[\zeta] = 0 \text{ for } \zeta < 0 \tag{9d}$$

Note that the preceding force depends on the normal component of the relative velocity between two particles. A similar viscous force which depends on the tangent relative velocity component is introduced in each intact element, for relative motion of the edge centered with respect to the body centered particle.

To damp the bulk deformation of individual particles, a viscous pressure is introduced with the functional form

$$P^{B(i)} = - c_1 \, \rho^{(i)} \, c_s^{(i)} \, h^{(i)} \, \dot{F}^{(i)} \tag{9e}$$

where c_1 is a dimensionless viscosity coefficient.

NUMERICAL CONDUCTION

As is standard in impact codes, a numerical heat conduction or artificial viscosity [30] is used in the present model. Given the use of entropy states in the Hamiltonian formulation, it takes the form

$$\dot{S}^{con(i)} = (1/\theta^{(i)}) \sum_{j=1}^{n} R^{(i,j)} (\theta^{(i)} - \theta^{(j)}) \tag{10a}$$

where $R^{(i,j)}$ is the numerical conduction coefficient

$$R^{(i,j)} = c_2 \, (1/2) \, (\rho^{(i)} \, c_s^{(i)} \, c_v^{(i)} \, A^{(i)} + \rho^{(j)} \, c_s^{(j)} \, c_v^{(j)} \, A^{(j)}) \; \Lambda[\zeta^{(i,j)}] \tag{10b}$$

with $c_v^{(j)}$ the specific heat for particle "i" and c_2 a dimensionless conduction coefficient.

MECHANICAL AND THERMAL CONSTRAINTS

The energy balance equation used in conventional continuum codes is replaced here by nonholonomic entropy evolution constraints for the particles

$$\dot{S}^{(i)} = \dot{S}^{irr(i)} - \dot{S}^{con(i)} \tag{11a}$$

where $\dot{S}^{irr(i)}$ is the entropy production rate due to viscous dissipation, plastic flow, and damage evolution

$$\dot{S}^{irr(i)} = (1 / \theta^{(i)}) \dot{W}^{(i)} \tag{11b}$$

$$\dot{W}^{(i)} = f^{(i)} \cdot \dot{c}^{(i)} - V_0^{(i)} P^{B(i)} \dot{F}^{(i)} + \Gamma^{(i)} \dot{D}^{(i)} + \eta^{(i)} \dot{d}^{(i)} + V_0^{e(i)} S^{(i)} : \dot{E}^P \tag{11c}$$

with $\dot{W}^{(i)}$ and $V_0^{(i)}$ the energy dissipation rate and reference volume for particle "i". As shown by Fahrenthold and Koo [16] in the hydrodynamic case, the Lagrange multipliers associated with these constraints are known, so that they introduce no new state variables. Similarly, the evolution equations for the plastic and damage variables are constraint equations which can be shown to introduce no new unknown Lagrange multipliers into the formulation.

Additional mechanical constraints are must be introduced to represent particle collisions. They are

$$|c^{(i)} - c^{(j)}| - \xi (h^{(i)} + h^{(j)}) \geq 0 \tag{12a}$$

where the constant ξ allows for close packing of the particles at the reference density. The value of ξ depends on the choice of relative sizes for the edge centered and body centered particles (for equal size $\xi = 0.879$). Since the preceding expression is an inequality constraint, it is represented in the model formulation process using the nonholonomic expressions

$$[(c^{(i)} - c^{(j)}) / |c^{(i)} - c^{(j)}|] \cdot (\dot{c}^{(i)} - \dot{c}^{(j)}) - \xi \{ h_0^{(i)} \dot{F}^{(i)} + h_0^{(j)} \dot{F}^{(j)} \} = 0$$

(12b)

where $h_0^{(i)}$ is the particle radius in the reference configuration. Since the Lagrange multipliers associated with the particle collision constraints are numerous, penalty forces $\lambda^{(i,j)}$ are introduced to impose the latter

$$\lambda^{(i,j)} = k^{(i,j)} [\xi (h^{(i)} + h^{(j)}) - |c^{(i)} - c^{(j)}|] \Lambda[\zeta^{c(i,j)}] \tag{12c}$$

where the step function ensures interaction of overlapping particles only

$$\zeta^{c(i,j)} = \xi (h^{(i)} + h^{(j)}) - |c^{(i)} - c^{(j)}|$$

(12d)

and $k^{(i,j)}$ is a penalty stiffness. For particles connected by springs in series

$$k^{(i,j)} = c_3 / [1.0/(K^{(i)} A_0^{(i)2} / V_0^{(i)}) + 1.0/(K^{(j)} A_0^{(j)2} / V_0^{(j)}] \tag{12e}$$

where $A_0^{(i)}$ is the reference cross sectional area for particle "i", and c_3 is a dimensionless penalty stiffness, while for parallel springs (as in DYNA3D)

$$k^{(i,j)} = c_3 (1/2) [K^{(i)} A_0^{(i)2} / V_0^{(i)} + K^{(j)} A_0^{(j)2} / V_0^{(j)}] \tag{12f}$$

(12f)

HAMILTON'S EQUATIONS

The preceding sections have defined the kinematics, stored energy functions, and constraints for the physical system. They lead to Hamilton's equations in the form

$$\dot{p}^{(i)} = -g^{(i)} - f^{(i)} + \sum_{j=1}^{n} \lambda^{(i,j)} (c^{(i)} - c^{(j)}) \; / \; |c^{(i)} - c^{(j)}| \tag{13a}$$

$$\dot{c}^{(i)} = m^{(i)-1} \, p^{(i)} \tag{13b}$$

$$\dot{H}^{(i)} = -G^{(i)} - V_o^{(i)} \, P^{B(i)} - \sum_{j=1}^{n} \xi \, h_o^{(i)} \, \lambda^{(i,j)} \tag{13c}$$

$$\dot{F}^{(i)} = J^{(i)-1} \, H^{(i)} \tag{13d}$$

$$\dot{S}^{(i)} = \dot{S}^{irr(i)} - \dot{S}^{con(i)} \tag{13e}$$

augmented by the evolution equations for the plastic strain and continuum damage variables. Integration of these nonlinear, history dependent relations for a chosen equation of state describes the thermomechanical dynamics of the impact problem of interest.

The state space model described here has been implemented in a three dimensional impact code [31], developed with a particular interest in orbital debris shielding applications. The state equations are integrated using a second order Runge-Kutta method, using time step limits described by Fahrenthold and Koo [16]. Currently Mie-Gruneisen and ideal gas equations of state are employed, and linked lists [32] are used to identify neighbor particles. The code incorporates compiler directives for parallel execution on Cray systems and SGI workstations. A pre-processor is included for model generation, as well as an automated rezoner which deletes particles moving outside a user specified control volume. The latter feature is essential for many orbital debris shielding simulations. Post processing is performed using commercial graphics software. Testing and further code development work is now in progress. The next section presents two example simulations, for which there are known experimental results.

EXAMPLE SIMULATIONS

The simulations discussed in this section employed material property data from Steinberg [25], and the following dimensionless coefficients:

$$c_o = c_1 = 0.01 \quad ; \quad c_2 = 0.1 \quad ; \quad c_3 = \alpha = \beta = 1.0 \quad ; \quad \xi = 0.900$$

The material failure stress in shear was set to the maximum yield stress, while the failure pressure in tension was set to the spall stress. The effective plastic strain at failure was set to 3.0.

The first example is an oblique Whipple shield impact simulation, at a velocity of seven kilometers per second. The problem parameters are provided in Table 1, and the simulation is depicted in Figures 1 and 2. Automated rezoning was used every 1,000 times steps to delete particles which move outside the modeled region above the wall plate. For the modeled aluminum materials, impact velocity, impact obliquity, shield and wall thickness, and standoff distance, experimental ballistic limit curves [33] predict failure of the wall plate for projectiles over 0.45 cm in diameter. The modeled projectile of 0.60 cm diameter clearly fails the wall plate, as shown in Figure 2, depicting the simulation results at 30.7 microseconds after impact. The required CPU time indicated in Table 1 is reasonable, for a three dimensional simulation. Note that the requirement to model fragmentation of the projectile, as well as contact-impact of all the projectile and shield fragments, presents significant difficulties for conventional Lagrangian codes. On the other hand, tracking small debris fragments requires a relatively fine Eulerian mesh,

Table 1. Oblique Whipple shield impact simulation

Projectile diameter (aluminum 6061-T6 sphere)   =   0.60 cm
Shield thickness (aluminum 6061-T6)   =   0.127 cm
Wall thickness (aluminum 6061-T6)   =   0.3175 cm
Shield-to-wall spacing   =   5.0 cm
Impact velocity   =   7.0 km/sec
Impact obliquity   =   15 degrees
Number of particles   =   207,363
Total simulation time   =   30.7 microseconds
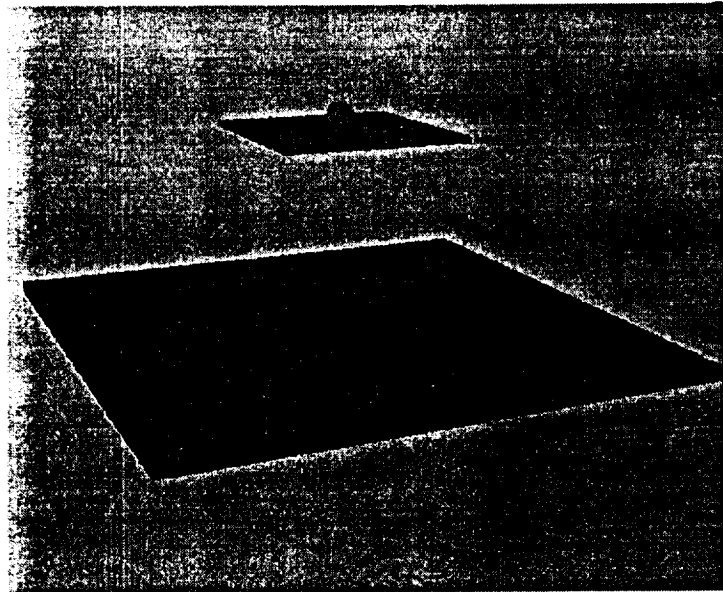Number of time steps   =   7,000
Wall clock time (2-CPU SGI Octane)   =   60 hours

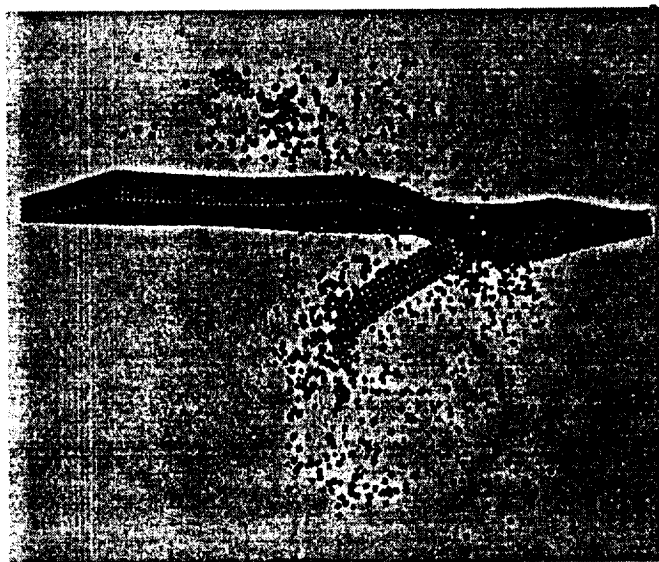Fig. 1. Oblique Whipple shield impact simulation (t = 0.0 microseconds).
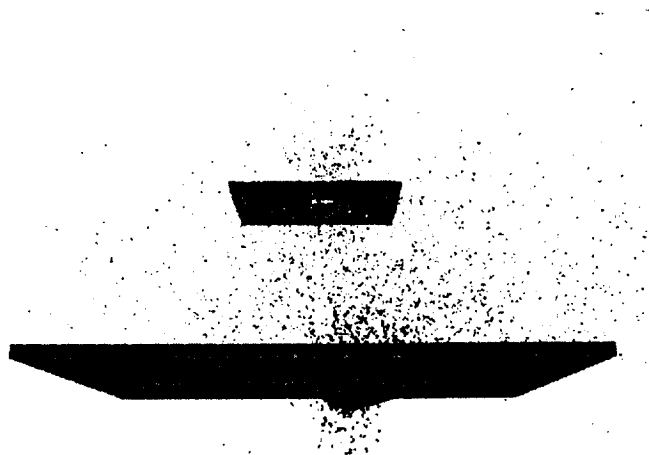
Fig. 2. Oblique Whipple shield impact simulation (t = 30.7 microseconds).

Table 2. Long rod impact simulation

Projectile diameter (DU 0.75% Ti cylinder)	=	0.767 cm
Projectile length	=	7.67 cm
Plate thickness (4340 steel)	=	0.64 cm
Projectile velocity	=	0.121 cm/μsec
Plate velocity	=	0.0217 cm/μsec
Impact obliquity	=	73.5 degrees
Number of particles	=	66,478
Total simulation time	=	100 μsec
Number of time steps	=	5,934
Wall clock time (6-CPU SGI Onyx)	=	7.50 hours
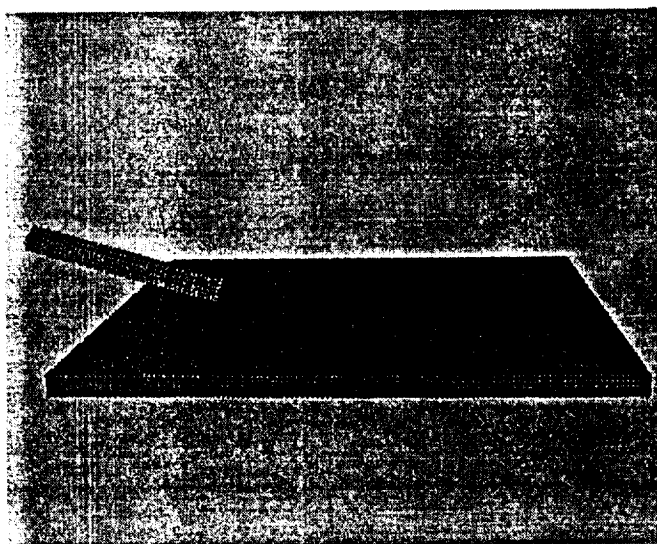
Fig. 3. Long rod impact simulation (t = 0.0 microseconds).

Fig. 4. Long rod impact simulation (half model at t = 100 microseconds).

computationally expensive in three dimensions. Hertel [6] reported a requirement of about 50 CPU hours on a Cray YMP for a three dimensional Whipple shield simulation using CTH, albeit at a standoff distance approximately twice that shown in this example. The latter simulation work incorporated significant user intervention, emphasizing the motivation for considering alternative methods in the simulation of shielding design problems.

The second example involves a highly oblique long rod impact on a flat plate, at projectile and target velocities of 1.21 and 0.217 kilometers per second. The problem parameters are provided in Table 2, and the simulation is depicted in Figures 3 and 4. This problem has been modeled with several codes, including CTH [34]. In the present case, pre-processor limitations did not allow for the hemispherical nose of the experimental projectile to be modeled, so a flat nose was represented. Figure 3 shows the projectile-target configuration at impact, while Figure 4 shows half the physical model (cut along the plane of symmetry) at 100 microseconds after impact. Experimental data at the latter time indicated an eroded rod length of 5.55 cm and a residual velocity of 1.069 kilometers per second. The present work yielded a residual rod length of 4.49 cm and a residual velocity of 0.950 kilometers per second. The corresponding CTH simulation yielded a better estimate of eroded rod length (6.00 cm) and residual velocity (0.956 kilometers per second). As in the first example, the CPU times reported for a parallel workstation in Table 2 and for a Cray YMP using CTH (4.02 hours) are not directly comparable. However the CPU time reported here is reasonable, for a relatively long (100 microsecond) impact simulation in three dimensions.

CONCLUSION

The present paper has outlined the development of a hybrid particle-finite element modeling approach to hypervelocity impact simulation. The method appears to have certain advantages over pure Lagrangian, Eulerian, and particle methods in the application of orbital debris shielding design. Although further development and testing of the method is in progress, comparisons of simulation results to representative hypervelocity impact problems show reasonable agreement with experiment. Recent research focused on Arbitrary Lagrangian-Eulerian (ALE), element-free Galerkin (EFG), Fluid Implicit Particle (FLIP), and other coupled or hybrid methods suggests that such methods will provide opportunities for the expanded use of simulation in the study of hypervelocity impact problems.

REFERENCES

1. J.J. Monaghan, Particle methods for hydrodynamics, *Computer Physics Reports*, 3, 71-124 (1985).

2. J.M. McGlaun, S.L. Thompson, and M.G. Elrick, CTH: a three dimensional shock wave physics code, *International Journal of Impact Engineering*, 10, 351-360 (1990).

3. J.O. Hallquist, Theoretical Manual for DYNA3D, Lawrence Livermore National Laboratories (1983).

4. E.L. Christiansen, J.L. Crews, J.E. Williamsen, J.H. Robinson, and A.M. Nolen, Enhanced meteoroid and orbital debris shielding, *International Journal of Impact Engineering*, 17, 217-228 (1995).

5. E.L. Christiansen and J.H. Kerr, Projectile shape effects on shielding performance at 7 Km/s and 11 Km/s, *International Journal of Impact Engineering*, 20, 165-172 (1997).

6. E.S. Hertel, Comparison of Analytic Whipple Bumper Shield Ballistic Limits with CTH Simulations, Sandia Report SAND92-0347 (1993).

7. E.P. Fahrenthold, A Lagrangian model for debris cloud dynamics simulation, *International Journal of Impact Engineering*, **14**, 229-240 (1993).

8. E.P. Fahrenthold, Oblique hypervelocity impact simulation for Whipple shield-protected structures, *International Journal of Impact Engineering*, **17**, 291-302 (1995).

9. R.J. Rabb and E.P. Fahrenthold, Numerical simulation of oblique impact on orbital debris shielding, *International Journal of Impact Engineering*, in press (1998).

10. G.R. Johnson, E.H. Petersen, and R.A. Stryk, Incorporation of an SPH option into the EPIC code for a wide range of high velocity impact computations, *International Journal of Impact Engineering*, **14**, 385-394 (1993).

11. K.G. Budge and J.S. Peery, RHALE: a MMALE shock physics code written in C++, *International Journal of Impact Engineering*, **14**, 107-120 (1993).

12. Y.Y. Lu, T. Belytschko, and M. Tabbara, Element-free Galerkin method for wave propagation and dynamic fracture, Computer *Methods in Applied Mechanics and Engineering*, **126**, 131-153 (1995).

13. D. Sulsky, Z. Chen, and H.L. Schreyer, A particle method for history dependent materials, *Computer Methods in Applied Mechanics and Engineering*, **118**, 179-196 (1994).

14. R.F. Stellingwerf C.A. and Wingate, Impact modeling with smooth particle hydrodynamics, *International Journal of Impact Engineering*, **14**, 707-718 (1993).

15. C.A. Wingate, R.F. Stellingwerf, R.F. Davidson, and M.W. Burkett, Models of high velocity impact phenomena, *International Journal of Impact Engineering*, **14**, 819-830 (1993).

16. E.P. Fahrenthold and J.C. Koo, Hamiltonian particle hydrodynamics, *Computer Methods in Applied Mechanics and Engineering*, **146**, 43-52 (1997).

17. E.P. Fahrenthold and J.C. Koo, Energy based particle hydrodynamics for hypervelocity impact simulation, *International Journal of Impact Engineering*, **20**, 253-264 (1997).

18. J.W. Swegle, D.L. Hicks, and S.W. Attaway, Smooth particle hydrodynamics stability analysis, *Journal of Computational Physics*, **116**, 123-134 (1995).

19. G.R. Johnson and S.R. Beissel, Normalized smoothing functions for SPH impact computations, *International Journal for Numerical Methods in Engineering*, **39**, 2725-2741 (1996).

20. D.J. Benson, Computational methods in Lagrangian and Eulerian hydrocodes, *Computer Methods in Applied Mechanics and Engineering*, **99**, 235-394 (1992).

21. T. Belytschko and J.I. Lin, A three-dimensional impact-penetration algorithm with erosion, *International Journal of Impact Engineering*, **5**, 111-127 (1987).

22. J.H. Ginsberg, Advanced Engineering Dynamics, Harper and Row, Inc., Cambridge (1988).

23. J. Lubliner, Plasticity Theory, Macmillan, New York (1990).

24. E.P. Fahrenthold and B.A. Horban, Thermodynamics of continuum damage and fragmentation models for hypervelocity impact, *International Journal of Impact Engineering*, **20**, 241-252 (1997).

25. D.J. Steinberg, Equation of State and Strength Properties of Selected Materials, Lawrence Livermore National Laboratory, Livermore, CA, UCRL-MA-106439 (1996).

26. L.D. Libersky, A.G. Petschenk, T.C. Carney, J.R. Hipp, and F.A. Allahdadi, High strain Lagrangian hydrodynamics, *Journal of Computational Physics*, **109**, 67-75 (1993).

27. S.A. Silling, CTH Reference Manual: Johnson-Holmquist Ceramic Model, Sandia National Laboratories, SAND92-0576 (1992).

28. W. Benz and E. Asphaug, Simulations of brittle solids using smooth particle hydrodynamics, *Computer Physics Communications*, **87**, 253-265 (1995).

29. E.P. Fahrenthold and C.H. Yew, Hydrocode simulation of hypervelocity impact fragmentation, *International Journal of Impact Engineering*, **17**, 303-310 (1995).

30. W.F. Noh, Errors for calculations of strong shocks using an artificial viscosity and an artificial heat flux, *Journal of Computational Physics*, **72**, 78-120 (1978).

31. E.P. Fahrenthold, User's Guide for EXOS, University of Texas at Austin (1998).

32. R.W. Hockney and J.W. Eastwood, Computer Simulation Using Particles, McGraw-Hill Inc., New York (1981).

33. E.L. Christiansen, Design and performance equations for advanced meteoroid and debris shields, *International Journal of Impact Engineering*, **14**, 145-156 (1993).

34. E.S. Hertel, A Comparison of the CTH Hydrodynamics Code With Experimental Data, Sandia Report SAND92-0347 (1992).

CHAPTER 3: WHIPPLE SHIELD SIMULATIONS

NUMERICAL SIMULATION OF OBLIQUE IMPACT ON ORBITAL DEBRIS SHIELDING

ROBERT J. RABB and ERIC P. FAHRENTHOLD

Department of Mechanical Engineering, University of Texas, Austin, TX 78712

Summary—Hybrid particle-finite element methods have been proposed as a modeling methodology well suited to the problem of hypervelocity impact simulation. To evaluate the use of such numerical methods for orbital debris shielding design, a series of simulations have been conducted using a three dimensional hybrid particle-finite element code now under development. Two sets of oblique impact simulations, one for a single bumper Whipple shield and one for a dual bumper or stuffed Whipple shield, have been compared to published ballistic limit equations, the latter derived from experiment. The results indicate that hybrid particle-finite element methods can provide an accurate and computationally tractable approach to the simulation of orbital debris shield performance.

INTRODUCTION

The design of high performance orbital debris shielding for space structures calls for the evaluation of a wide range of new shielding materials and geometry's. In particular, multi-plate geometry's and composite materials appear to offer significant performance improvements over conventional aluminum Whipple shields, using a protection per unit areal weight metric [1]. To date most research on the shielding design problem has been pursued experimentally. However several factors motivate the development of improved computer aided design tools: (1) promising new materials and shield geometry's have greatly expanded the number of candidate shielding designs, (2) the relatively complex interaction of impact velocity, impact obliquity, and material failure effects means that a rather large number of experiments are needed to fully characterize the three dimensional performance of any single design concept, (3) the desire for faster, cheaper spacecraft design places increased emphasis on simulation as opposed to experiment, and (4) the range of impact velocities and kinetic energies of interest goes beyond the capabilities of conventional light gas guns.

Although experimental research will continue to occupy a critical role in orbital debris shield design, improved computer codes tailored to address the orbital debris impact problem are expected to assume a larger role. Experience to date has shown that conventional Eulerian and Lagrangian hydrocodes are not ideally suited to this simulation task [2, 3], in particular where oblique impact (fully three dimensional) simulations are concerned. Pure particle methods are well suited to three dimensional modeling of the debris propagation portion of the shielding design problem. However their rather approximate treatment of material strength effects can introduce uncertainties in predicting the spacecraft structural response (fracture, spallation, etc.). The latter response can be strongly dependent on strength and material history effects, especially where "near ballistic limit" simulations are concerned.

Recognizing the advantages of particle methods in debris propagation calculations and the sensitivity of the structural response simulation to material strength effects, some code development research has been directed at coupled particle-finite element codes [4] or hybrid particle-finite element methods for use in the simulation of hypervelocity impact. The present paper describes the application of one hybrid particle-finite element method, described in detail by

Fahrenthold and Horban [5], to the specific problem of orbital debris shield design. A series of three dimensional simulations involving oblique impact on single and multi-plate aluminum shields has been performed for comparison to published experimental ballistic limit curves. The results of these simulations demonstrate the utility of particle-finite element methods in the development of a new computer codes tailored to the orbital debris shielding design problem.

NUMERICAL MODELING OF ORBITAL DEBRIS SHIELDING

Space structures face a current and perhaps growing threat of impact with orbiting space debris. For example, inspections of the Space Shuttle orbiters often reveal some impact damage. The frequency of these impacts suggests that the population of small orbital debris is increasing, due to both spacecraft breakups and collisions among existing orbital debris fragments. For long lived space structures, including low earth orbit satellites and the International Space Station (ISS), the probability of a serious impact is significant. The greatest danger arises from fragments one millimeter to one centimeter in length, with a density of 2.8 gm/cc and impact velocities as high as 13 km/s. Larger fragments exist, but the probability of a collision with debris over one centimeter in size is remote [6]. As a result, the focus of much shielding design work, as well as the present simulation work, has been on sub-centimeter sized aluminum particle impacts over the aforementioned velocity range.

Most orbital shielding design research has been experimental, with analytical and numerical modeling playing a secondary role. There are a number of factors which make numerical simulation of oblique impact on orbital debris shielding a very demanding computational problem: (1) equation of state and anisotropic strength models are needed for new composite shielding materials, (2) better "material failure" models are needed for both composite and metallic shields, (3) conventional Lagrangian, Eulerian, and particle codes can be difficult to apply effectively, and (4) computer resource requirements are very large. The large memory and CPU time requirements are due to: (1) oblique impact (three dimensional) effects, (2) large differences in problem characteristic lengths (ratio of shield thickness to standoff distance), (3) a wide range of material effects and corresponding time scales (shock thermodynamics govern shield perforation, while plasticity and fracture govern structural failure of the wall plate), and (4) fluid-structure interaction effects present in pressurized vessel impacts.

The complexity of the numerical modeling problem can appreciated by considering the simplest case of a conventional Whipple shield impact. The simulation problem can be subdivided into three phases. The first phase is shield perforation, a "hydrodynamic" event in which material strength effects are secondary. The second phase is a debris transport calculation, a non-continuum problem which demands very general contact-impact models. The third phase is the wall plate impact simulation, where material strength effects are critical and structural failure may occur relatively slowly. No single Eulerian, particle-based, or Lagrangian code is ideally suited to simulate all three phases of the problem.

Lagrangian finite element codes normally model perforation by "eroding" elements [7], often discarding the internal energy of eroded elements and attaching the eroded element mass to neighboring nodes. Their slideline-based contact-impact algorithms can lack the generality needed for debris cloud transport calculations, and mesh distortion can mandate frequent rezoning. On the positive side, Lagrangian finite element codes provide very accurate material strength models.

Eulerian finite difference (finite volume) codes model perforation as a hydrodynamic event, providing a robust characterization of multi-material impact, at the cost of complex mixed-cell thermodynamics and interface tracking algorithms. An inordinately fine mesh may be required to model debris transport [8]. Finally, strength modeling is approximate, since in general a different collection of material can contribute to the calculation of local material history data at each time step.

Smooth particle hydrodynamic (SPH) codes [9-12] use "Lagrangian" particles but an "Eulerian" internal energy. They provide a very general characterization of contact-impact, although conventional SPH density calculations imply a multi-material mixing effect which is usually ignored. Particle models are ideal for debris transport calculations, but some problems have been experienced with tensile and boundary instabilities [13]. In addition, SPH modeling of strength effects is approximate: different material particle sets can contribute to the calculation of local material history data at each time step, and numerical "fracture" can occur when particles lose contact.

Recognizing the tremendous accomplishments of pure Eulerian (e.g. CTH [14]), Lagrangian (e.g. DYNA3D [15]), and particle (e.g. SPHINX [16]) codes, the preceding discussion suggests nonetheless that some hybrid formulation may be advantageous for oblique debris shield impact simulations. One possibility is some combination of particle and finite element methods - the particle capability can simulate shield perforation and debris transport while the finite element capability can simulate strength dependent (near ballistic limit) effects during the wall plate impact. Published work in this area has emphasized adding SPH options to finite element codes [4]. The questions which arise with such an approach include: (1) are conventional erosion and slideline algorithms sufficiently general? and (2) how will particle-element interactions and element-to-particle transition be represented? The answers to these questions will determine in part the range of contact-impact problems which can be efficiently modeled using this approach.

As an alternative approach, another hybrid particle-finite element formulation has been developed which combines the Lagrangian particle dynamics method of Fahrenthold and Koo [17, 18] with a large strain elastic-plastic finite element formulation. This method, described in detail by Fahrenthold and Horban [5], has been implemented in a three dimensional computer code (EXOS) developed for the simulation of hypervelocity impact on orbital debris shielding. The code can simulate the large strain, elastic-plastic, thermomechanical impact dynamics of solid, fluid, or combined solid-fluid structures and systems. The code is particle based, with a finite element based strength model, and uses a Mie-Gruneisen equation of state. The kinematics, energy functions, and constraints are fully Lagrangian in form. The formulation includes finite strain plasticity, scalar damage variables, decoupled volumetric-deviatoric response, and transient thermal dynamics. The code is three dimensional and includes a plane of symmetry option. A pre-processor simplifies model generation. Although the code is currently undergoing additional development, it has been used to perform the simulations discussed in the sections which follow.

It should be noted here that a number of relatively new numerical modeling techniques including Arbitrary Lagrangian-Eulerian (ALE) methods [19], element free Galerkin methods [20], and alternative particle methods [21] are under development which may prove effective in addressing the orbital debris simulation problem. However to date these methods have not been extensively applied to the application of interest here.
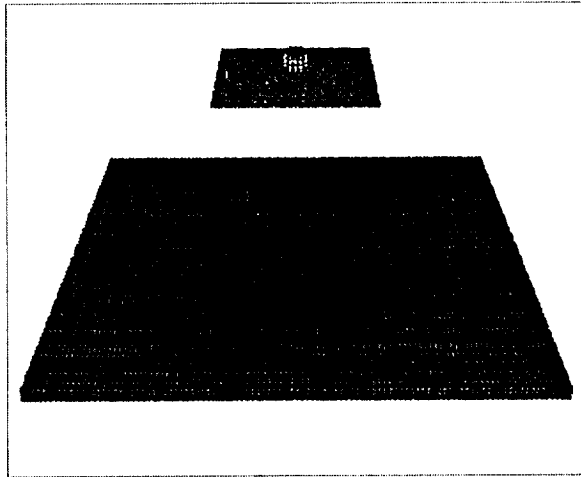

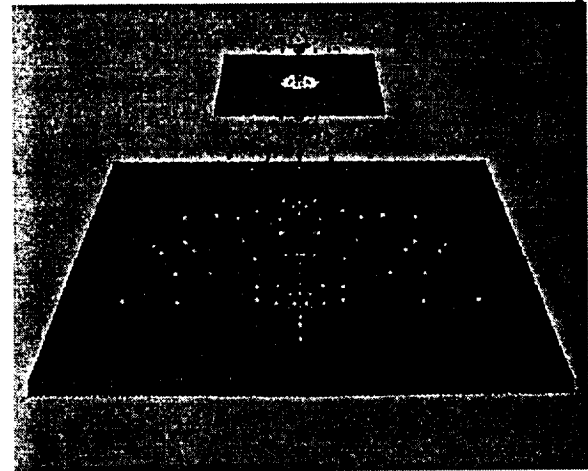Fig. 1. Example oblique Whipple shield impact simulation (t = 0 microseconds).

Fig. 2. Example oblique Whipple shield impact simulation (t = 33 microseconds).

SIMULATION METHODOLOGY

As an illustration of the simulations discussed in the sections that follow, Figures 1 and 2 depict the results of a typical oblique Whipple shield impact simulation. The parameters of this example simulation are provided in Table 1 (material properties were taken from Steinberg[22]). The example involves the 7 km/sec impact of a 0.60 cm diameter aluminum sphere on an aluminum Whipple shield and wall plate combination, at an impact obliquity of 15 degrees. Figures 1 and 2 are plots of the simulation results at 0 and 33 microseconds after impact respectively. Consistent with the experimentally derived ballistic limit curve of Christiansen [1], the simulation predicts

perforation of the wall plate. The simulation involved approximately 30,000 particles and required approximately 10 CPU hours on a high performance workstation. Automated rezoning was used every 500 time steps to minimize CPU time (particles moving outside a user specified region above the wall plate were zoned out of the calculation).

Table 1. Example oblique Whipple shield impact simulation		
Projectile diameter (aluminum sphere)	=	0.60 cm
Shield thickness (aluminum)	=	0.127 cm
Wall thickness (aluminum)	=	0.3175 cm
Shield-to-wall spacing	=	5.0 cm
Impact velocity	=	7.0 km/sec
Impact obliquity	=	15 degrees
Equation of state type	=	Mie-Gruneisen
Spall stress	=	0.012 Mbar
Failure pressure (tension)	=	0.012 Mbar
Yield stress	=	0.0029 Mbar
Plastic failure strain	=	3.0
Shear modulus	=	0.271 Mbar
Density	=	2.7 g/cc
Melt temperature	=	1,220 degrees K
Number of particles	=	29,422
Total simulation time	=	33 microseconds
Number of time steps	=	4,500
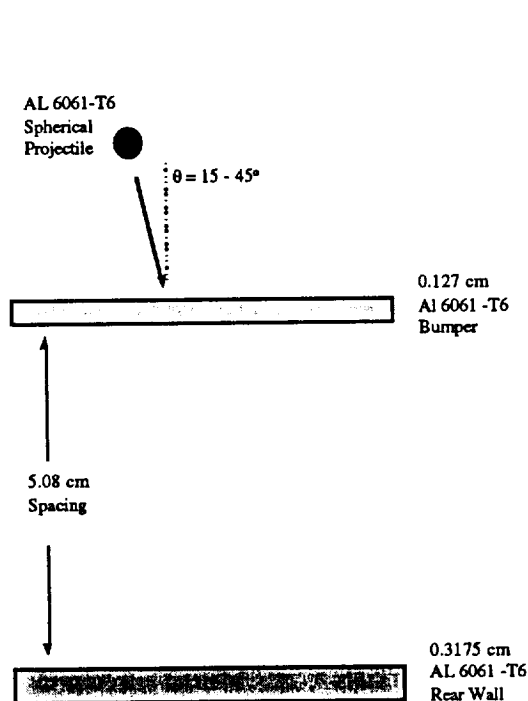
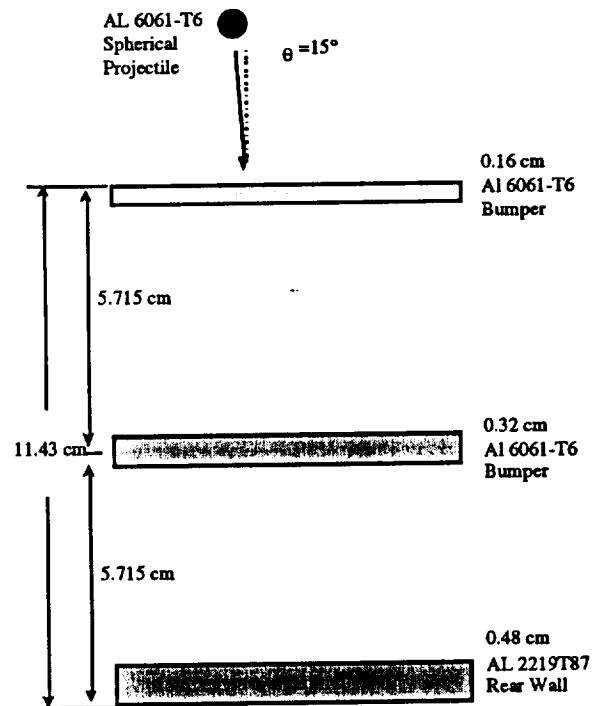Fig. 3. Geometry for the Whipple shield ballistic limit simulations.

Fig. 4. Geometry for the multi-plate shield ballistic limit simulations.

In order to conduct a systematic evaluation of the utility of hybrid particle-finite element methods in orbital debris shield design, a series of simulations like the one just described were performed, in an attempt to match several experimentally derived ballistic limit curves. Such ballistic limit curves portray graphically the critical projectile diameter required to fail a specific shield and wall plate configuration, as a function of projectile velocity and impact obliquity. Failure is defined as perforation or spall of the wall plate. Ballistic limit curves have been constructed by testing a wide variety of shield geometry's and materials, and are used extensively in orbital debris shield design.

The next section discusses the results of a series of Whipple shield (Figure 3) impact simulations performed at impact obliquity's of 15 and 45 degrees, for various projectile diameters and impact velocities. The results are compared to known ballistic limit curves derived from experiment. In the section which then follows, the results of several simulations involving all-aluminum stuffed Whipple shields (Figure 4) are compared to corresponding experiments and a published ballistic limit curve for a weight equivalent composite-aluminum stuffed Whipple shield. The final section notes the conclusions of this study and plans for future work.

WHIPPLE SHIELD BALLISTIC LIMIT SIMULATIONS

The Whipple shield is the basis for most simple orbital debris shielding designs. The Whipple shield is a thin, sacrificial sheet of material (a bumper) mounted at a fixed standoff distance from the protected structure. An incoming projectile hits the bumper and hopefully fragments or melts, distributing its impact momentum over a wide area of the rear wall. Experiments on aluminum have shown the existence of three distinct projectile response regimes, based on the normal component of the projectile impact velocity. The first regime is located below 3 km/s. At low velocities, the projectile remains nearly intact after impact with the bumper. Shock pressures are low, so the rear wall suffers impact from a deformed but sound projectile. Hence in this regime the critical particle diameter decreases as velocity increases. The second (intermediate) velocity regime is between 3 and 7 km/s. In this velocity range, the projectile fragments and/or melts on impact, reducing its lethality as its velocity increases. The third region consists of normal velocities above 7 km/s, wherein the debris cloud that impacts the rear wall is a multiphase mixture of projectile and bumper components. In this regime the debris cloud becomes more damaging as the impact velocity increases. The solid lines in Figures 5 and 6 are experimental ballistic limit curves [1] for the Whipple shield configuration of Figure 3, for impact obliquity's of 15 and 45 degrees respectively.

Numerical impact simulations were performed for the Whipple shield configuration of Figure 3, for ten different projectile diameter and impact velocity combinations, at each of the two aforementioned obliquity's, in an attempt to match the experimental ballistic limit curves of Figures 5 and 6. In particular, simulations were conducted for projectile diameters slightly smaller and slightly larger than the critical diameter, at velocities of 3, 5, 7, 9, and 11 km/s. In general the code was run to a stop time 6-15 times that required for an unimpeded projectile traveling at the initial velocity to traverse the space between the shield and rear wall. This allowed sufficient time for the debris cloud to impact the rear wall and generate an impulse load. Due to the large number of simulations required and the large CPU time requirements of three dimensional simulation, relatively coarse models of less than 10,000 particles were initially used. In those cases where the coarse models failed to match the ballistic limit curves, finer models (up to 40,000 particles) were used in an attempt to improve the simulation results. CPU times for the coarse and fine models were approximately 20 and 67 CPU hours respectively, on a Cray J90. Particle count and CPU time for each simulation are detailed by Rabb [23]. The simulation results are shown by the open and closed triangles plotted in Figures 5 and 6, indicating good agreement, except at the highest velocity in the 15 degree obliquity case. Tables 2 and 3 describe the wall plate damage predicted by the simulation, including bulging, spallation, and/or perforation.

MULTI-PLATE SHIELD SIMULATIONS

One relatively new system designed to improve spacecraft protection from orbital debris is the multi-plate or stuffed Whipple shield. The simplest stuffed Whipple shield improves upon the basic Whipple by adding an intermediate layer of material between the rear wall and the aluminum bumper (Figure 4). This intermediate layer may be aluminum or a composite material, such as
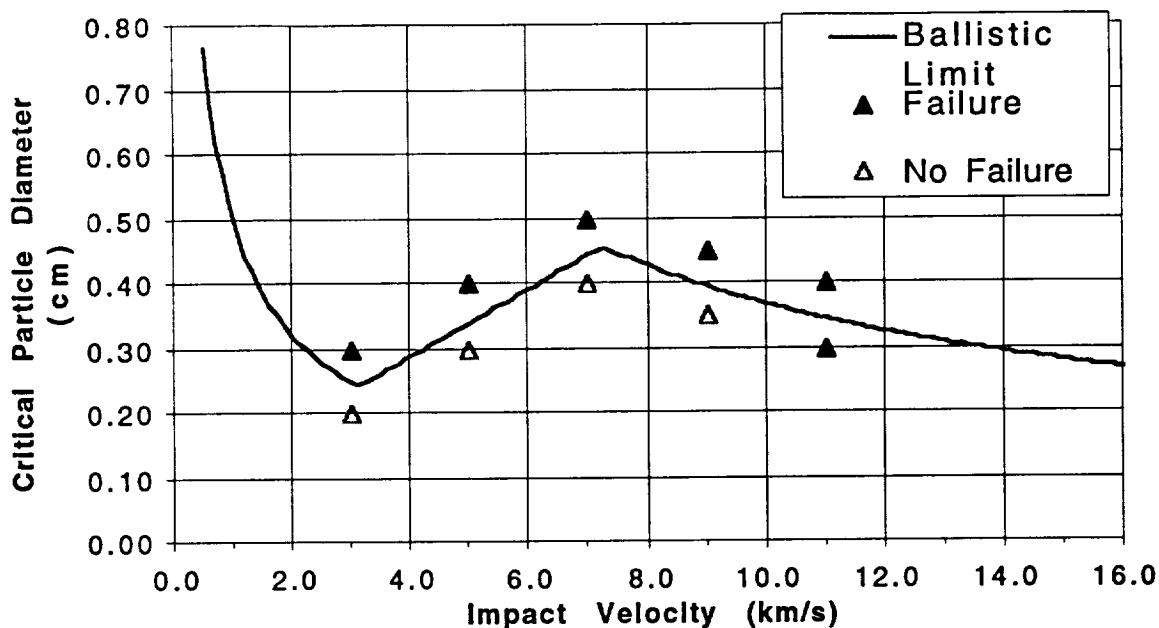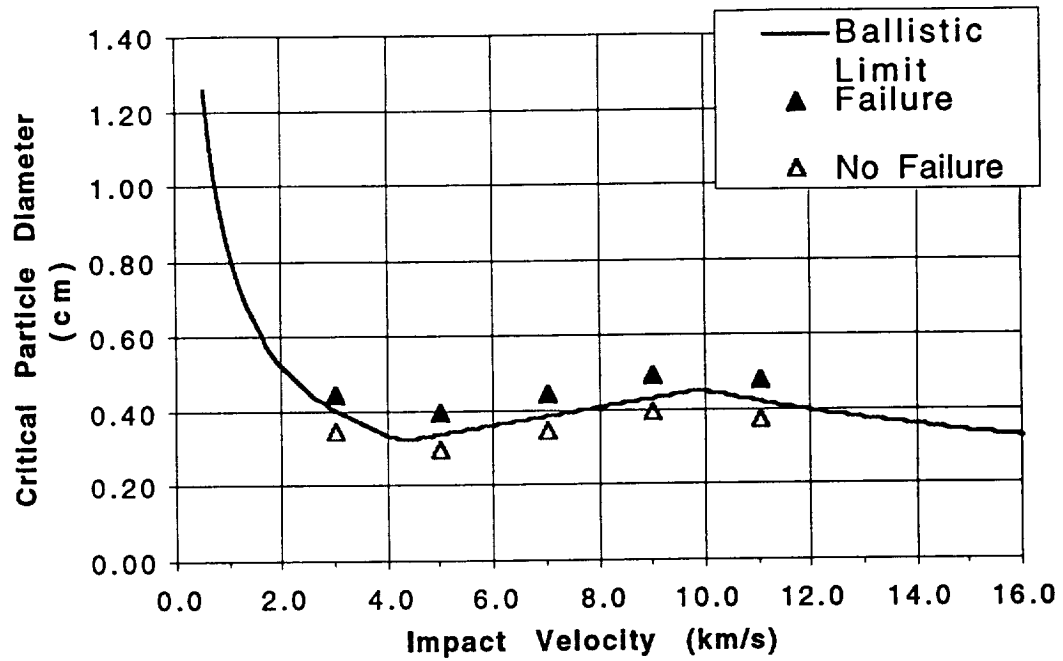
Fig. 5. Ballistic limit curve for the 15 degree obliquity Whipple shield simulations.

Table 2. Predicted damage for the 15 degree obliquity Whipple shield simulations (velocity in km/sec, projectile diameter in cm)

Velocity (diameter)	Shield Failure	Rear Wall Damage Description
3 (0.20)	No	Slight bulge (1 mm deep)
3 (0.30)	Yes	Spallation
5 (0.30)	No	Slight bulge (1 mm deep)
5 (0.40)	Yes	Spallation; Bulge (2 mm deep)
7 (0.40)	No	Slight bulge (2 mm deep)
7 (0.50)	Yes	Perforation; Hole (17 mm diam)
9 (0.35)	No	Slight bulge (2 mm deep)
9 (0.45)	Yes	Spallation; Bulge (25 mm diam, 9 mm deep)
11 (0.30)	Yes	Perforation; Hole (5 mm diam)
11 (0.40)	Yes	Spallation; Bulge (12 mm diam, 2 mm deep)

Fig. 6. Ballistic limit curve for the 45 degree obliquity Whipple shield simulations.

Table 3. Predicted damage for the 45 degree obliquity Whipple shield simulations (velocity in km/sec, projectile diameter in cm)

Velocity (diameter)	Shield Failure	Rear Wall Damage Description
3 (0.35)	No	Slight bulge (1 mm deep)
3 (0.45)	Yes	Spallation
5 (0.30)	No	Slight bulge (2 mm deep)
5 (0.40)	Yes	Spallation
7 (0.35)	No	Slight bulge (2 mm deep)
7 (0.45)	Yes	Perforation; Bulge (2 mm deep)
9 (0.40)	No	Slight bulge (1 mm deep)
9 (0.50)	Yes	Spallation; Bulge (3 mm deep)
11 (0.375)	No	Slight bulge (1 mm deep)
11 (0.425)	Yes	Spallation; Bulge (18 mm diam, 3 mm deep)

combination of Nextel and Kevlar. The intermediate layer can generate additional shocks in the projectile and disrupt the moving debris cloud, rendering it less lethal when it reaches the rear wall [24, 25]. Although the additional shield does contribute particles to the debris cloud, these particles are normally much smaller than the projectile fragments. Experiments have shown that the benefits of the intermediate layer outweigh its disadvantages.

Ballistic limit equations for the stuffed Whipple shield are not as well developed as those for simple Whipple shields. However Christiansen and Kerr [25] do provide ballistic limit equations for a specific Nextel-Kevlar-MLI (Multi-Layer Insulation) stuffed Whipple configuration which is of potential interest for ISS shielding applications. The solid line in Figure 7 shows that ballistic limit curve, for a projectile impact obliquity of 15 degrees. The latter authors also cite several experiments on weight equivalent all-aluminum stuffed Whipple shields, demonstrating the superior performance of the composite design. Figure 4 shows the weight equivalent all-aluminum stuffed Whipple shield used in the cited experiments.

In the interest of evaluating the particle-finite element modeling methodology used here on a stuffed Whipple shield configuration, three simulations were performed for the all-aluminum shield configuration of Figure 4, at an impact obliquity of 15 degrees, attempting to duplicate the cited experimental results. The results were also compared to the weight equivalent Nextel-Kevlar-MLI ballistic limit curve shown in Figure 7. No simulations were performed for Nextel-Kevlar-MLI stuffed Whipple designs, due to the lack of equation of state data for the composite materials and the fact that the required anisotropic strength models for the composite materials are still under development [26].

The solid triangles in Figure 7 indicate the projectile diameters and velocities for which simulations were conducted. The simulations were run for 61-66 microseconds, approximately four times that required for an unimpeded projectile traveling at the initial velocity to traverse the space between the first shield and the rear wall. Approximately 35,000 particles were employed, with each simulation requiring about 23 CPU hours on a Cray J90. Each of the simulations predicted similar results, namely slight bulging and spallation failure of the wall plate. The latter results are generally consistent with the experimental data, in that two of the three experiments showed wall plate failure. Note from Figure 7 that the tested velocities and projectile diameters varied only slightly between the three tests. In addition, the simulations indicate that the performance of all-aluminum stuffed Whipple shields is inferior to that of weight-equivalent composite designs, given the predicted failures of the wall plate at particle diameters below the experimental Nextel-Kevlar-MLI ballistic limit curve shown in Figure 7. It should be noted that due to CPU time constraints, the simulations were terminated after the first indication of wall plate failure (spallation). The debris cloud of projectile and bumper particles had not in all cases fully loaded the rear wall. The rear wall could incur additional damage from subsequent loading of the traveling debris.
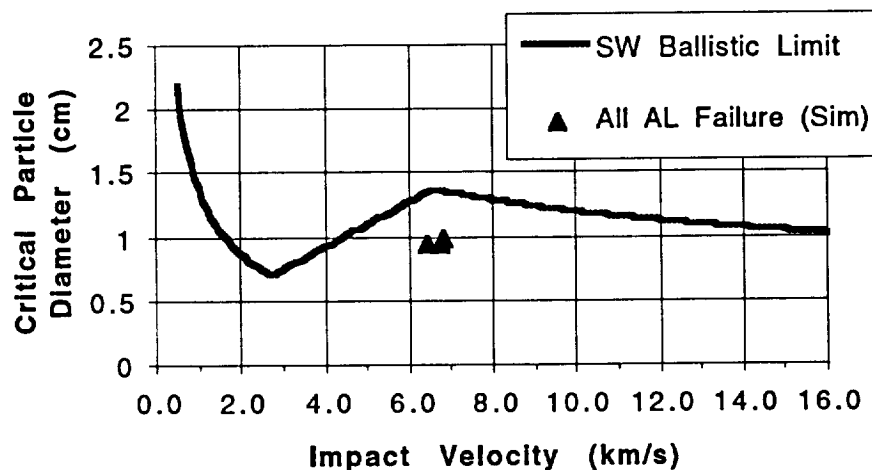

Fig. 7. Ballistic limit curve for the 15 degree obliquity multi-plate shield simulations.

CONCLUSIONS

The present paper has described the application of a new particle-finite element modeling method in the simulation of hypervelocity impact on orbital debris shielding. Three dimensional simulation results were compared to experimentally derived ballistic limit curves for oblique impact on Whipple and multi-plate spacecraft shielding, at velocities ranging from 3 to 11 km/s. In general the simulations show good agreement with the experimental curves, suggesting the further development of coupled or hybrid particle-element methods for hypervelocity impact simulation.

Although the simulation results presented here are encouraging, they represent preliminary work involving a new code and a new numerical modeling scheme. Since the present simulations were evaluated using a fail/no-fail criterion only, the accurate simulation of failure modes was not critically evaluated. In addition, the Mie-Gruneisen equation of state used here is certainly approximate at the high end of the impact velocity range considered. Relatively coarse models were employed, refined somewhat whenever initial simulation results were not consistent with the experimental curves. All of these issues warrant further study.

Additional code verification and testing is needed, as well as development and implementation work on composite equation of state and anisotropic strength models for new shielding designs. However the results presented here do support a trend towards the increased use of computer simulation in orbital debris shield design. Until experimental capabilities are developed to reach all velocities and impact energies of interest, simulations will provide the only estimates of shield performance in some hypervelocity impact regimes.

REFERENCES

1. E.L. Christiansen, Design and performance equations for advanced meteoroid and debris shields, *International Journal of Impact Engineering*, **14**, 145-156 (1993).
2. E.P. Fahrenthold, A Lagrangian model for debris cloud dynamics simulation, *International Journal of Impact Engineering*, **14**, 229-240 (1993).
3. E.P. Fahrenthold, Oblique hypervelocity impact simulation for Whipple shield-protected structures, *International Journal of Impact Engineering*, **17**, 291-302 (1995).
4. G.R. Johnson, E.H. Petersen, and R.A. Stryk, Incorporation of an SPH option into the EPIC code for a wide range of high velocity impact computations, *International Journal of Impact Engineering*, **14**, 385-394 (1993).
5. E.P. Fahrenthold and B.A. Horban, A hybrid particle-finite element method for hypervelocity impact simulation, *International Journal of Impact Engineering*, in press.
6. W.M. Isbell and W.J. Tedeschi, Hypervelocity research and the growing problem of space debris, *International Journal of Impact Engineering*, **14**, 359-372 (1993).
7. T. Belytschko and J.I. Lin, A three-dimensional impact-penetration algorithm with erosion, *International Journal of Impact Engineering*, **5**, 111-127 (1987).
8. E.S. Hertel, Comparison of Analytic Whipple Bumper Shield Ballistic Limits with CTH Simulations, Sandia Report SAND92-0347 (1993).
9. J.J. Monaghan, An Introduction to SPH, *Computer Physics Communications.*, **48**, 89-96 (1988).
10. R.F. Stellingwerf and C.A. Wingate, Impact modeling with smooth particle hydrodynamics, *International Journal of Impact Engineering*, **14**, 707-718 (1993).
11. L.D. Libersky, A.G. Petschenk, T.C. Carney, J.R. Hipp, and F.A. Allahdadi, High strain Lagrangian hydrodynamics, *Journal of Computational Physics*, **109**, 67-75 (1993).
12. W. Benz and E. Asphaug, Simulations of brittle solids using smooth particle hydrodynamics, *Computer Physics Communications*, **87**, 253-265 (1995).
13. G.R. Johnson and S.R. Beissel, Normalized smoothing functions for SPH impact computations, *International Journal for Numerical Methods in Engineering*, **39**, 2725-2741 (1996).
14. J.M. McGlaun, S.L. Thompson, and M.G. Elrick, CTH: a three dimensional shock wave physics code, *International Journal of Impact Engineering*, **10**, 351-360 (1990).
15. J.O. Hallquist, Theoretical Manual for DYNA3D, Lawrence Livermore National Laboratories (1983).

16. C.A. Wingate, R.F. Stellingwerf, R.F. Davidson, and M.W. Burkett, Models of high velocity impact phenomena, *International Journal of Impact Engineering*, **14**, 819-830 (1993).
17. E.P. Fahrenthold and J.C. Koo, Hamiltonian particle hydrodynamics, *Computer Methods in Applied Mechanics and Engineering*, **146**, 43-52 (1997).
18. E.P. Fahrenthold and J.C. Koo, Energy based particle hydrodynamics for hypervelocity impact simulation, *International Journal of Impact Engineering*, **20**, 253-264 (1997).
19. K.G. Budge and J.S. Peery, RHALE: A MMALE shock physics code written in C++, *International Journal of Impact Engineering*, **14**, 107-120 (1993).
20. Y.Y. Lu, T. Belytschko, and M. Tabbara, Element-free Galerkin method for wave propagation and dynamic fracture, *Computer Methods in Applied Mechanics and Engineering*, **126**, 131-153 (1995).
21. D. Sulsky, Z. Chen, and H.L. Schreyer, A particle method for history dependent materials, *Computer Methods in Applied Mechanics and Engineering*, **118**, 179-196 (1994).
22. D.J. Steinberg, <u>Equation of State and Strength Properties of Selected Materials</u>, Lawrence Livermore National Laboratory, Livermore, CA, UCRL-MA-106439 (1996).
23. R.J. Rabb, <u>Numerical Simulation of Ballistic Limit Curves for Orbital Debris Shielding</u>, Master of Science thesis, Department of Mechanical Engineering, University of Texas at Austin (1998).
24. E.L. Christiansen, J.L. Crews, J.E. Williamsen, J.H. Robinson, and A.M. Nolen, Enhanced meteoroid and orbital debris shielding, *International Journal of Impact Engineering*, **17**, 217-228 (1995).
25. E.L. Christiansen and J.H. Kerr, Projectile shape effects on shielding performance at 7 Km/s and 11 Km/s, *International Journal of Impact Engineering*, **20**, 165-172 (1997).
26. E.P. Fahrenthold and B.A. Horban, Hypervelocity impact simulation in composite materials, *Proceedings of the 5th International Conference on Composites Engineering*, Las Vegas, 275-276 (1998).

CHAPTER 4: OTHER EXAMPLE SIMULATIONS

..

EXAMPLE SIMULATIONS

using the hypervelocity impact code

EXOS

Eric P. Fahrenthold, University of Texas at Austin

The following simulations illustrate application of the hypervelocity impact code EXOS (Fahrenthold, 1998), developed at the University of Texas at Austin under the support of the Hypervelocity Impact Technology Facility (HIT-F) at NASA Johnson Space Center and the State of Texas Advanced Technology Program.

The first example involves a highly oblique long rod impact on a flat plate, at projectile and target velocities of 1.21 and 0.217 kilometers per second. The problem parameters are provided in Table 1, and the simulation is depicted in Figures 1a through 1d (all figures show half the physical model, cut along the plane of symmetry). This problem has been simulated with several codes, including CTH (Hertel, 1992). Figure 1a shows the projectile-target configuration at impact, while Figures 1b and 1c show the simulation results at 50 at 100 microseconds after impact. Experimental data at the latter time indicated an eroded rod length of 5.55 cm and a residual velocity of 1.069 kilometers per second. The present work yielded a residual rod length of 5.4 cm and a residual velocity of 1.0 kilometers per second. The corresponding CTH simulation (Hertel, 1992) yielded a somewhat less accurate estimate of eroded rod length (6.00 cm) and residual velocity (0.956 kilometers per second).

The second example involves oblique impact of an aluminum sphere on a flat plate at a velocity of 6.56 kilometers per second. The problem parameters are provided in Table 2, and the simulation is depicted in Figures 2a through 2d. Note that unlike Eulerian and SPH (Smooth Particle Hydrodynamics) models, the present true Lagrangian formulation makes an unambiguous prediction regarding the hole size in the plate (Figure 2c). An areal density plot produced from the simulation (Figure 2d) shows good agreement with the radiograph of the corresponding experiment, the latter reported by Piekutowski (1996).

The third example involves a pair of oblique Whipple shield impact simulations, at a velocity of 7.0 kilometers per second. The problem parameters are provided in Table 3, and the simulations are depicted in Figures 3a through 3d. For the modeled aluminum materials, impact velocity, impact obliquity, shield and wall thickness, and standoff distance, experimental ballistic limit curves (Christiansen, 1993) predict failure of the wall plate for projectiles over about 0.50 cm in diameter. The modeled projectile of 0.40 cm diameter deforms but does not perforate the wall plate, as shown in Figure 3b, depicting the simulation results at 54 microseconds after impact. On the other hand, the modeled projectile of 0.60 cm diameter clearly fails the wall plate, as shown in Figure 3d, again at 54 microseconds after impact. Note that the requirement to model fragmentation of the projectile, as well as contact-impact of all the projectile and shield fragments, presents significant difficulties for conventional Lagrangian codes. On the other hand, tracking small debris fragments requires a very fine Eulerian mesh, computationally very expensive in three dimensions (Hertel, 1993). The latter simulation work also incorporated significant user intervention, emphasizing the motivation for considering alternative methods in the simulation of shielding design problems. With regards to SPH methods, poor strength modeling generally makes accurate characterization of the wall plate ballistic limit extremely difficult (Faraud et al., 1998). It appears that no EFG (Element Free Galerkin) based work has attempted to simulate an impact and penetration problem as complex as this example (Belytschko et al., 1996).
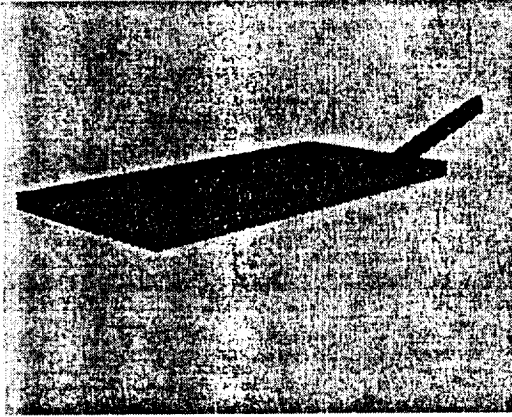
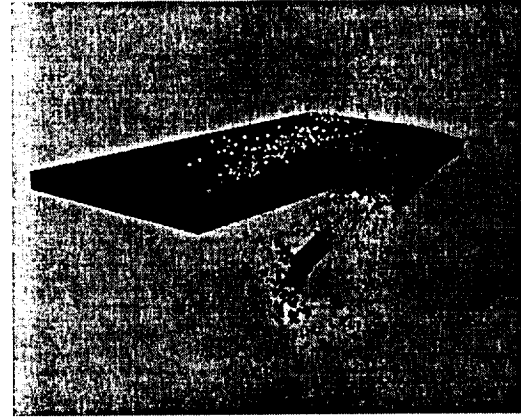Figure 1a. Oblique long rod impact, color on velocity (t = 0 microseconds).

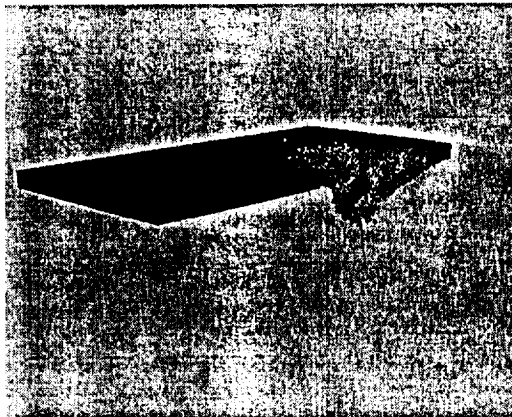Figure 1c.Oblique long rod impact, color on temperature (t = 100 microseconds).

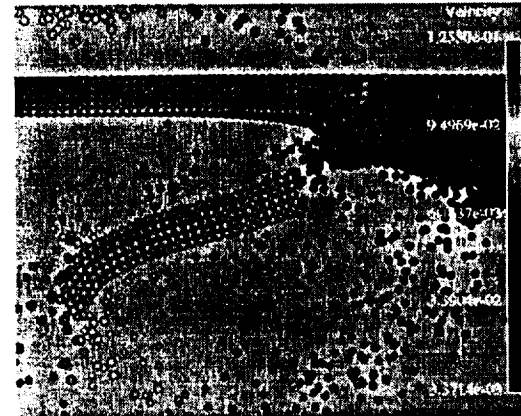Figure 1b. Oblique long rod impact, color on temperature (t = 50 microseconds).

Figure 1d. Oblique long rod impact, color on velocity (t = 100 microseconds).

Table 1: Oblique long rod impact simulation

Projectile diameter (DU 0.75% Ti cylinder)	=	0.767 cm
Projectile length	=	7.67 cm
Plate thickness (4340 steel)	=	0.64 cm
Projectile velocity	=	1.21 km/sec
Plate velocity	=	0.217 km/sec
Impact obliquity	=	73.5 degrees
Equation of state	=	Mie-Gruneisen
Number of particles	=	66,478
Total simulation time	=	100 microseconds
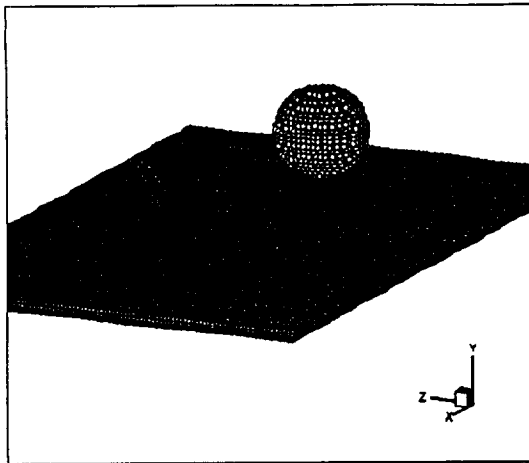
Figure 2a. Oblique sphere impact, color on material (t = 0.0 microseconds).
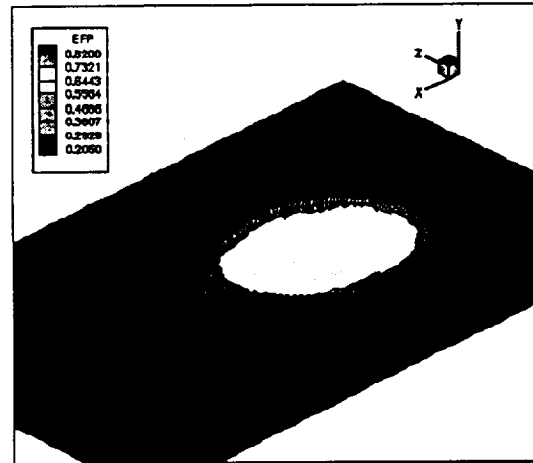
Figure 2c. Plate perforation, color on plastic strain (t = 6.6 microseconds).
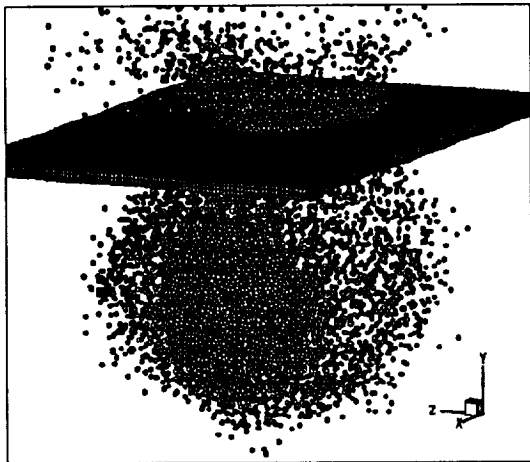

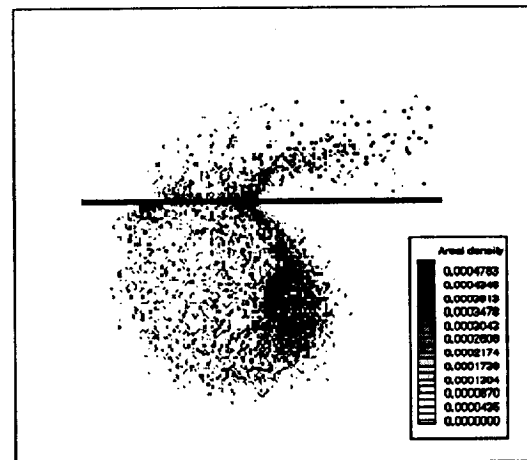Figure 2b. Oblique sphere impact, color on material (t = 6.6 microseconds).

Figure 2d. Oblique sphere impact, greyscale on areal density (t = 6.6 microseconds).

Table 2: Oblique plate impact simulation

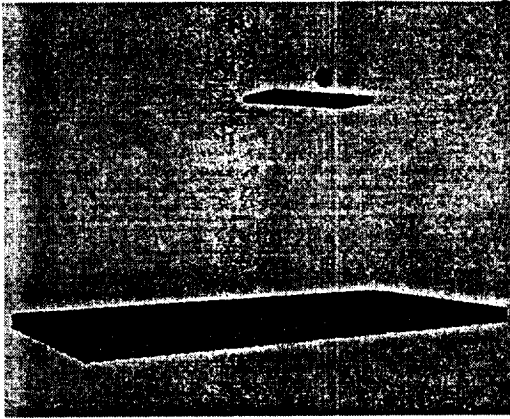|		
Projectile diameter (aluminum sphere)	=	0.953 cm
Plate thickness (aluminum)	=	0.1143 cm
Impact velocity	=	6.56 km/sec
Impact obliquity	=	45 degrees
Equation of state	=	SESAME 3718
Number of particles	=	33,146
Total simulation time	=	6.6 microseconds

Figure 3a. Oblique Whipple shield
impact, projectile below ballistic limit size
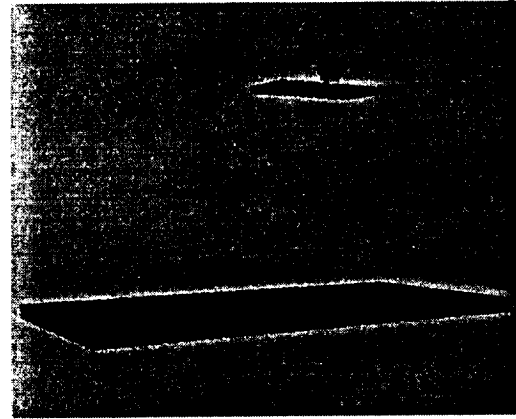(t = 0 microseconds).

Figure 3c. Oblique Whipple shield
impact, projectile above ballistic limit size
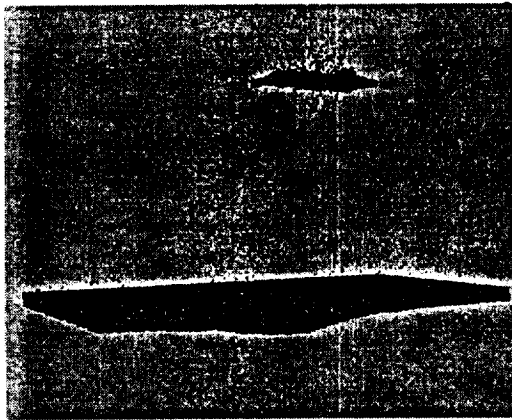(t = 0 microseconds).

Figure 3b. Oblique Whipple shield
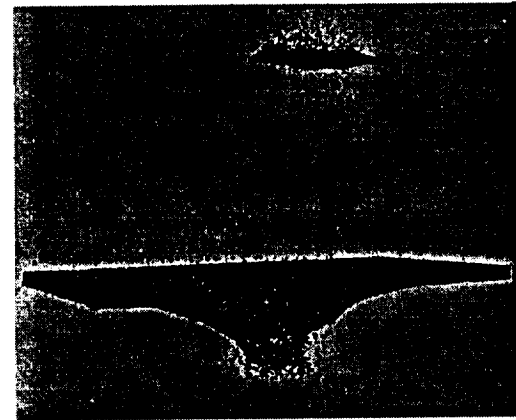impact, projectile below ballistic limit size
(t = 54 microseconds).

Figure 3d. Oblique Whipple shield
impact, projectile above ballistic limit size
(t = 54 microseconds).

Table 3: Oblique Whipple shield impact simulations

Projectile diameters (aluminum spheres)	=	0.40 & 0.60 cm
Shield thickness (aluminum)	=	0.127 cm
Wall thickness (aluminum)	=	0.3175 cm
Shield to wall spacing	=	5.0 cm
Impact velocity	=	7.0 km/sec
Impact obliquity	=	15 degrees
Equation of state	=	SESAME 3718
Number of particles	=	109,000
Total simulation time	=	54 microseconds

The fourth example represents a simulation of Southwest Research Institute test number 7139-6, which involved a multi-plate shield. The problem parameters are provided in Table 4, and the simulation is depicted in Figures 4a through 4c. The figures show the simulation results at 74.0 microseconds after impact.

TABLE 4. Multi-plate shield impact simulation

Projectile mass (hollow cylinder)	=	1.06g
Impact velocity	=	11.18 km/sec
Impact obliquity	=	65 degrees
Shield thickness (aluminum)	=	0.16002 cm
Wall #1 thickness (aluminum)	=	0.3175 cm
Wall #2 thickness (aluminum)	=	0.2032 cm
Shield-to-wall #1 spacing	=	6.096 cm
Wall #1-to-wall #2 spacing	=	2.53 cm
Equation of state type	=	SESAME 3718
Failure strain	=	1.00
Number of particles	=	216,106
Total simulation time	=	74.0 microseconds

The simulation shows no wall plate failure, as observed in the experiment. Hole sizes may be compared as follows (all dimensions in centimeters):

	Experiment	Simulation
Shield #1:	7.62 x 4.45	4.5 x 3.0 (approximate)
Shield #2:	5.72 x "narrow"	3.0 x 3.0 (approximate)
Wall plate:	no failure	bulge, no failure

The preceding results could perhaps be improved by reducing the strength of the inhibited shaped charge projectile, which was modeled here as a hollow sphere of intact aluminum.
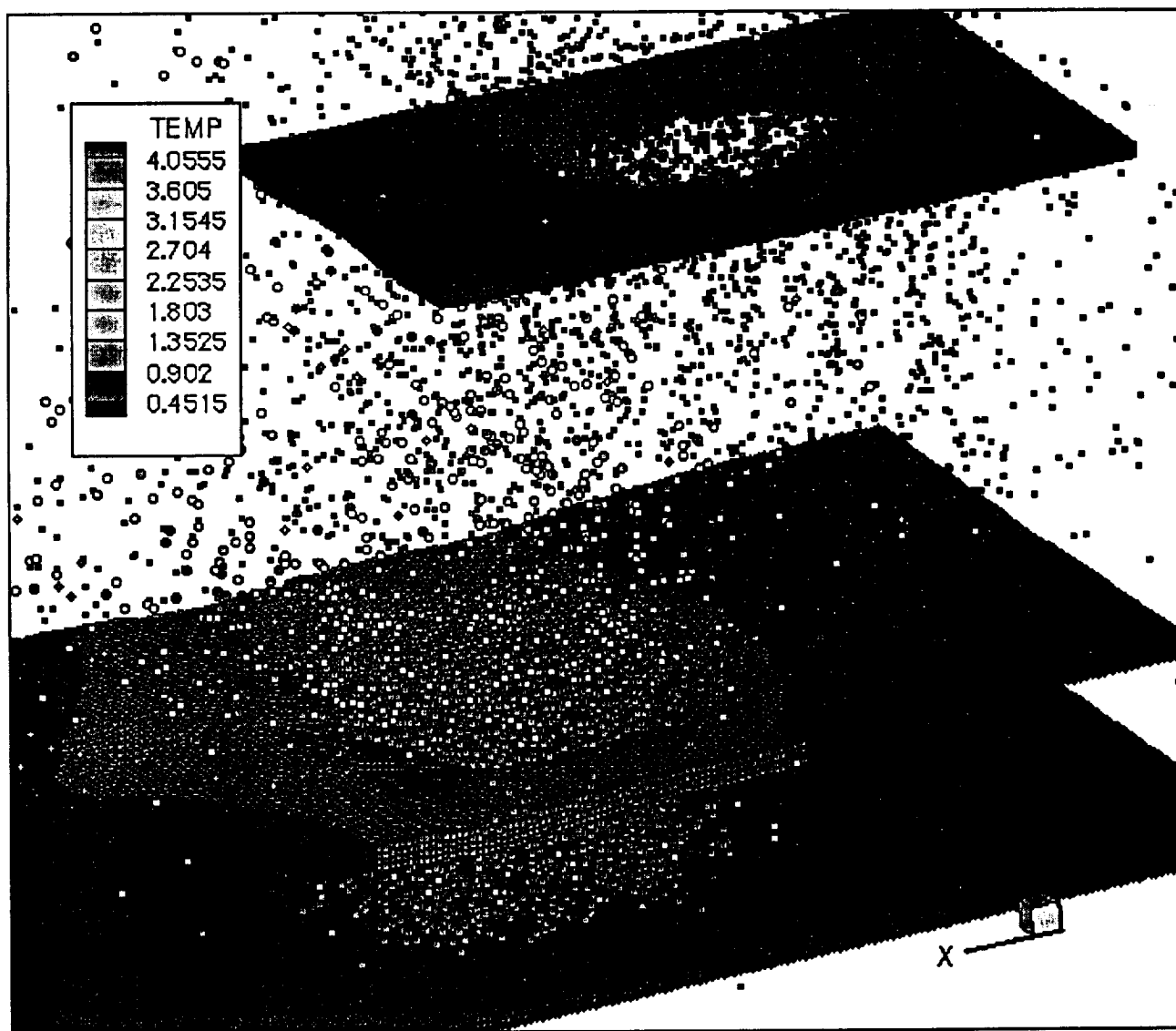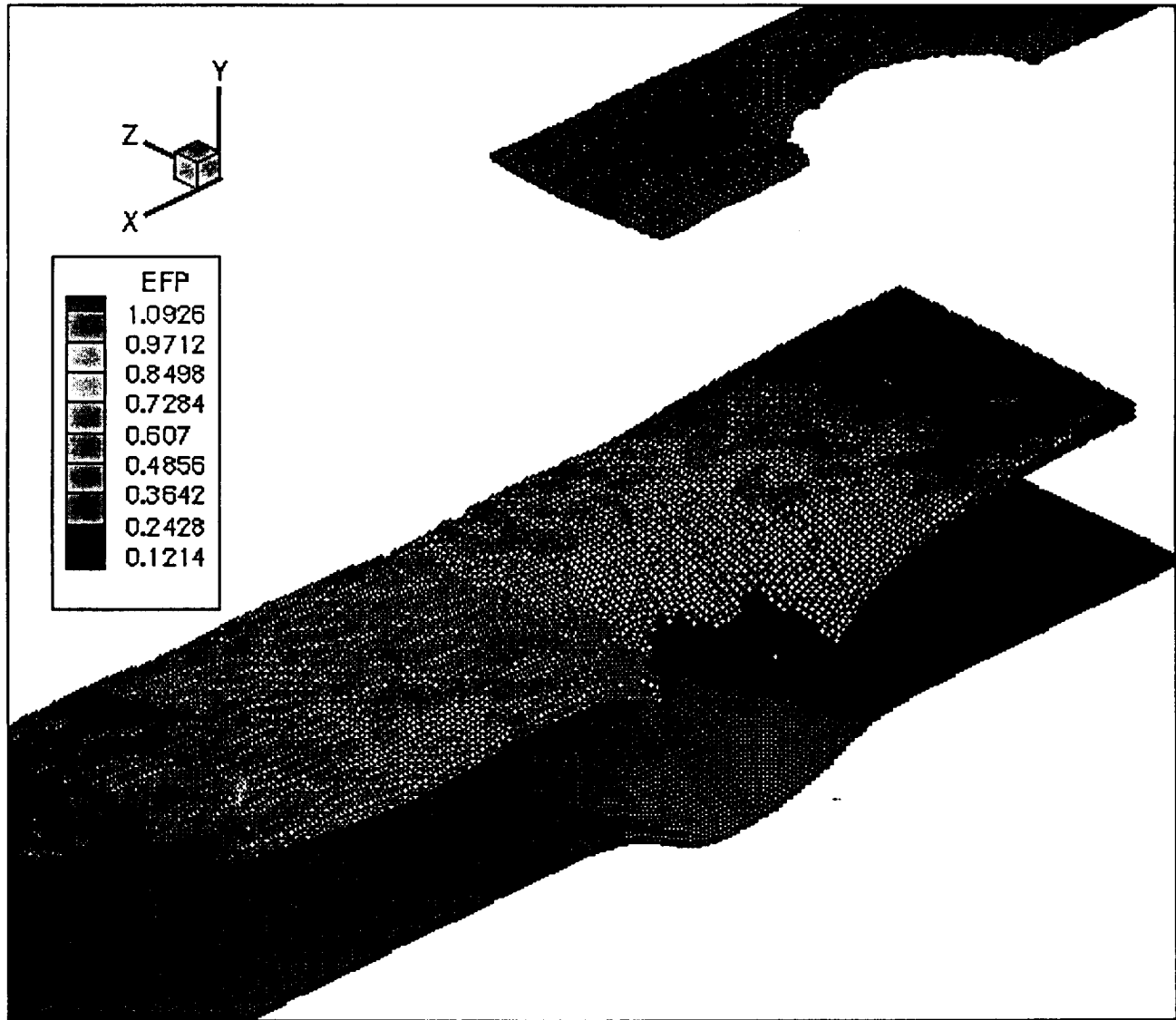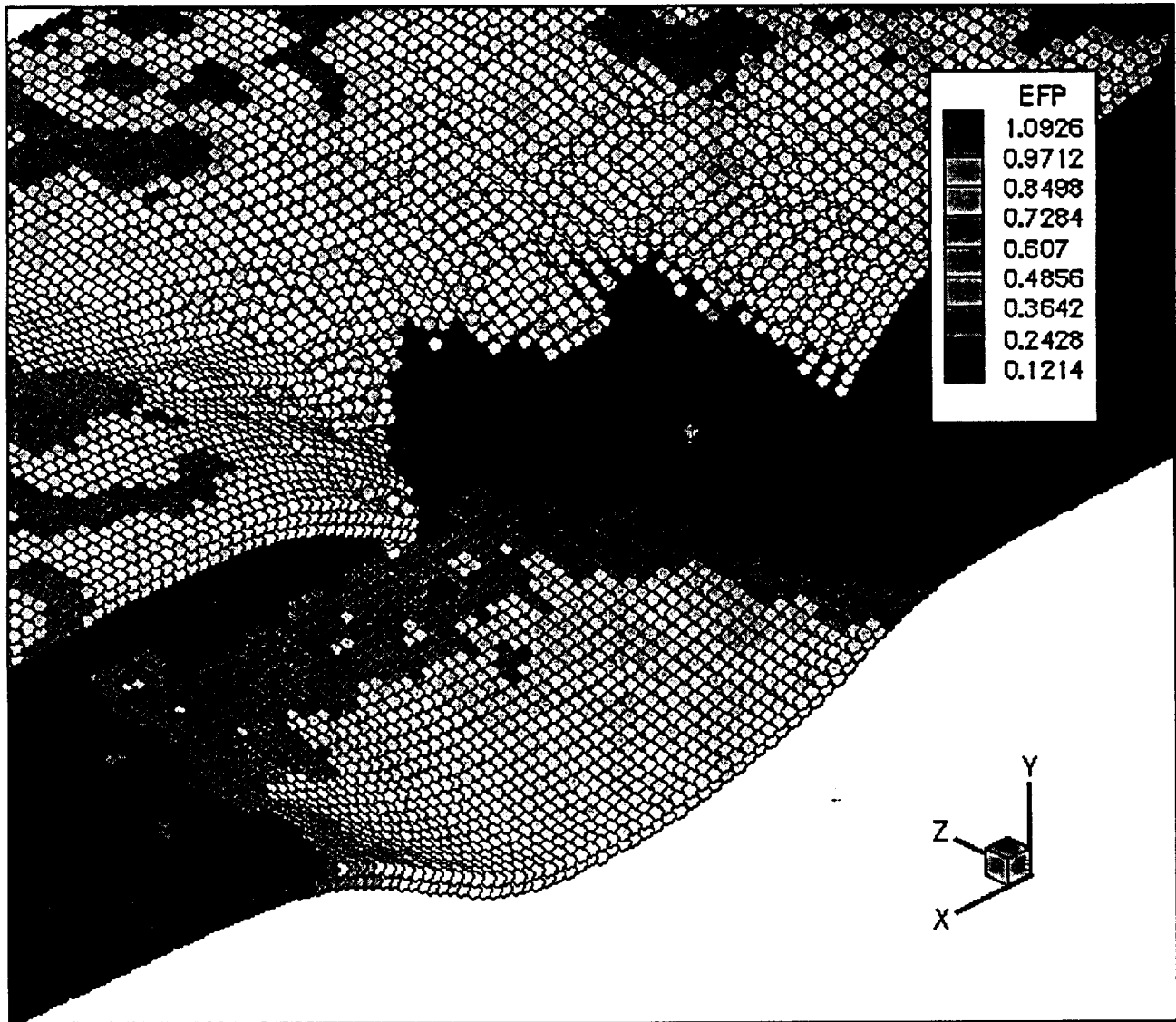
Figure 4a.

Figure 4b.

Figure 4c.

REFERENCES

Belytschko, T., Krongauz, Y., Organ, D., Fleming, M., and Krysl, P., 1996, "Meshless Methods: A Overview and Recent Developments," *Computer Methods in Applied Mechanics and Engineering*, Vol. 139, pp. 3-47.

Christiansen, E.L., 1993, "Design and Performance Equations for Advanced Meteoroid and Debris Shields," *International Journal of Impact Engineering*, Vol. 14, pp. 145-156.

Fahrenthold, E.P., 1998, User's Guide for EXOS, University of Texas at Austin.

Faraud, M., Destefanis, R., Palmieri, D., and Marchetti, M., 1998, "SPH Simulations of Debris Impacts Using Two Different Computer Codes," *International Journal of Impact Engineering*, in press.

Hertel, E.S., 1992, "A Comparison of the CTH Hydrodynamics Code With Experimental Data," Sandia Report SAND92-0347.

Hertel, E.S., 1993, "Comparison of Analytic Whipple Bumper Shield Ballistic Limits with CTH Simulations," Sandia Report SAND92-0347.

Piekutowski, A.J., 1996, " Formation and Description of Debris Clouds Produced by Hypervelocity Impact," NASA Contractor Report 4707.

CHAPTER 5: CONCLUSION

This report has described work performed under NASA Grant NAG9-946, including the development and validation of a new particle-element method for hypervelocity impact simulation. Future work is aimed at extension of the method to include more complex materials and more complex shielding designs.